Journal of Physics and Chemistry of Solids 93 (2016) 40–51

Contents lists available at ScienceDirect

Journal of Physics and Chemistry of Solids

journal homepage: www.elsevier.com/locate/jpcs

Cohesive properties of (Cu,Ni)–(In,Sn) intermetallics: Database, electron-density correlations and interpretation of bonding trends

S.B. Ramos [a,b,*], N.V. González Lemus [a,b], G.F. Cabeza [c,d], A. Fernández Guillermet [e,f]

[a] Facultad de Ingeniería, Universidad Nacional del Comahue, Buenos Aires 1400, 8300 Neuquén, Argentina
[b] Instituto de Investigación y Desarrollo en Ingeniería de Procesos, Biotecnología y Energías Alternativas – CONICET-UNCo, Argentina
[c] Dpto. de Física, Universidad Nacional del Sur, Bahía Blanca, Argentina
[d] Instituto de Física – UNS-CONICET, Argentina
[e] Centro Atómico Bariloche e Instituto Balseiro, Avda. Bustillo 9500, 8400 Bariloche, Argentina
[f] CONICET, Argentina

ARTICLE INFO

Article history:
Received 22 December 2015
Accepted 20 January 2016
Available online 22 January 2016

Keywords:
Intermetallics compounds
Ab initio calculations
Electronic structure
Thermodynamic properties

ABSTRACT

This paper presents a systematic and comparative study of the composition and volume dependence of the cohesive properties for a large group of Me–X intermetallic phases (IPs) with Me=Cu,Ni and X=In, Sn, which are of interest in relation with the design of lead-free soldering (LFS) alloys. The work relies upon a database with total-energy *versus* volume information developed by using projected augmented waves (PAW) calculations. In previous papers by the current authors it was shown that these results account satisfactorily for the direct and indirect experimental data available. In the present work, the database is further expanded to investigate the composition dependence of the volume (V_0), and the composition and volume dependence of the bulk modulus (B_0) and cohesive energy (E_{coh}). On these bases, an analysis is performed of the systematic effects of replacing Cu by Ni in several Me–X phases (Me=Cu,Ni and X=In,Sn) reported as stable and metastable, as well as various hypothetical compounds involved in the thermodynamic modeling of IPs using the Compound-Energy Formalism. Moreover, it is shown that the cohesion-related quantities $(B_0/V_0)^{1/2}$ and $(E_{coh}^{1/2}/V_0)$ can be correlated with a parameter expressing the number of valence electrons per unit volume. These findings are compared in detail with related relations involving the Miedema empirical electron density at the boundary of the Wigner–Seitz cell. In view of the co-variation of the cohesive properties, E_{coh} is selected as a key property and its composition and structure dependence is examined in terms of a theoretical view of the bonding which involves the hybridization of the *d*-states of Cu or Ni with the *s* and *p*-states of In or Sn, for this class of compounds. In particular, a comparative analysis is performed of the DOS of various representative, isostructural Me–X compounds. Various effects of relevance to understand the consequences of replacing Cu by Ni in LFS alloys are highlighted and explained microscopically for the first time.

1. Introduction

A long-standing challenge of the research work in the physics and chemistry of materials is the accurate account of the theoretically and practically relevant properties for metallic alloys and compounds. This problem has stimulated the development of specific databases with information on various types of properties, in particular, those involved in the design of new materials. In principle, information about the structural, cohesive and thermodynamic quantities might be obtained from direct measurements. However, a fully experimental characterization is usually produced only for some selected compositions and conditions of temperature and pressure. As a consequence, there has been considerable interest in the design and testing of phenomenological and theoretical methods to produce and systematize the information on the thermophysical properties of technically interesting systems.

The theme of the present study is the application of *ab initio*, density-functional-theory techniques, to study the structural and cohesive properties of the intermetallic phases (IPs) occurring in alloys of the Cu–In, Cu–Sn, Ni–In and Ni–Sn systems. These systems have been investigated in connection with the design of lead-free soldering (LFS) alloys and are here studied to provide

* Corresponding author at: Instituto de Investigación y Desarrollo en Ingeniería de Procesos, Biotecnología y Energías Alternativas – CONICET-UNCo, Buenos Aires 1400, 8300 Neuquén, Argentina.
E-mail address: susana.ramos@fain.uncoma.edu.ar (S.B. Ramos).

http://dx.doi.org/10.1016/j.jpcs.2016.01.017
0022-3697/

Table 1
Calculated cohesive energy, equilibrium atomic volume and bulk modulus for the elements Cu, Ni, In, and Sn. The cohesive energy is given in kJ/mol, the equilibrium volume (V_0) in Å^3/atom and the bulk modulus (B_0) in GPa. The valence electron density (n_{VED}) and the electron density at the boundary of the Wigner–Seitz cell (n_{WS}) are given in units of 4.6 10^{22} electrons cm^{-3}, following Miedema's approach.

Phase	E_{coh}	V_0	B_0	n_{VED}	n_{WS}
Ni (cF4)	495.126	(10.931	186.2)[a]	19.888	5.36
	428.000[b]	(11.026	197.0)[c]		
		(10.940	201.4)[d]		
			187.6[e]		
Cu (fcc)	338.938	(12.020	142.3)[f]	19.894	3.18
	336.000[b]	11.625[g]	142.0[h]		
In (tI2)	233.096	(27.505	36.5)[a]	2.371	1.6
	243.000[b]	(27.417	35.7)[d]		
		26.020[i]	(41.8)[j]		
Sn (tI4)	309.382	(28.348	48.6)[a]	3.067	1.9
	303.000[b]	26.886[i]	57.9[k]		

[a] Ab initio PAW GGA calculations [5].
[b] Experimental data at 0 K [47].
[c] Ab initio US-PP GGA calculations [37].
[d] Ab initio FP-LAPW GGA calculations [38].
[e] Experimental data at 0 K [39].
[f] Ab initio GGA calculations [40].
[g] Experimental data extrapolated at 0 K [41,42].
[h] Experimental data at 0 K [43].
[i] Experimental data [44].
[j] Experimental data at 293 K [45].
[k] Experimental data at 4.2 K [46].

Table 2
Calculated cohesive energy, equilibrium atomic volume and bulk modulus for stable, metastable, ideal and hypothetical Cu–In intermetallic phases. The cohesive energy is given in kJ/mol-atom, the equilibrium volume (V_0) in Å^3/atom and the bulk modulus (B_0) in GPa. The valence electron density (n_{VED}) and the electron density at the boundary of the Wigner–Seitz cell (n_{WS}) are given in units of 4.6 10^{22} electrons cm^{-3}, following Miedema's approach.

Phase	at% In	E_{coh}	V_0	B_0	n_{VED}	n_{ws}
Stable						
Cu_7In_3 (aP40)	30	308.620	(15.096	99.3)[a]	12.384	2.524
			14.695[b]			
Cu_9In_4 (cP52)	30.8	306.353	(15.143	101.1)[a]	12.258	2.509
			14.477[b]			
$Cu_{10}In_7$ (mC68)	41	297.280	(16.841	86.2)[a]	9.947	2.319
			16.251[c]			
$Cu_{11}In_9$ (mC20)	45	292.330	(17.369	81.5)[a]	9.262	2.248
			16.697[b]			
$CuIn_2$ (tI12)	66.7	268.738	(20.506	62.6)[a]	6.007	1.925
			19.782[d]			
Ideal						
Cu_2In (hP6)	33.3	296.265	(15.534	92.1)[a]	11.662	2.461
CuIn (hP4)	50	283.772	(19.415	76.3)[a]	7.838	2.165
$CuIn_2$ (hP6)	66.7	253.332	(22.131	49.9)[a]	5.566	1.925
Hypothetical						
Cu_4In (cF16)	20	308.916	14.514[a]		13.480	2.722
Cu_3In (oP8)	25	311.949	14.488[a]		13.504	2.622
Cu_5In_4 -η_1 (mP36)	44.44	293.170	17.873[a]		9.055	2.258
Cu_5In_4 -η_2 (mC54)	44.44	293.017	17.889[a]		9.047	2.258
Cu_6In_5 -η (mC44)	45.45	291.800	18.144[a]		8.823	2.241

[a] *Ab initio* PAW GGA calculations [4].
[b] Experimental data [44].
[c] Experimental data [13].
[d] Experimental data [11].

complementary information and analysis that can be useful for practical and theoretical aims.

The experimental data available at present is insufficient and does not allow a comparative study of the thermodynamic properties of stable intermetallic phases in these systems, as well as to analyze trends and correlations based on their compositions. Additionally, theoretical information obtained can be of value in

Table 3
Calculated cohesive energy, equilibrium atomic volume and bulk modulus for stable, metastable, ideal and hypothetical Cu–Sn intermetallic phases. The cohesive energy is given kJ/mol-atom, the equilibrium volume (V_0) in Å^3/atom and the bulk modulus (B_0) in GPa. The valence electron density (n_{VED}) and the electron density at the boundary of the Wigner–Seitz cell (n_{WS}) are given in units of 4.6 10^{22} electrons cm^{-3}, following Miedema's approach.

Phase	at% In	E_{coh}	V_0	B_0	n_{VED}	n_{ws}
Stable						
Cu_4Sn (cF16)	20	326.030	(14.726	99.6)[a]	13.655	2.755
			14.312[b]			
$Cu_{10}Sn_3$ (hP26)	23	331.739	(14.506	109.4)[a]	14.064	2.703
			14.074[b]			
Cu_3Sn (oP8)	25	331.900	(14.701	104.2)[a]	13.678	2.670
			(13.590	132.2)[c]		
			14.052[b]			
Cu_3Sn (oP80)	25	331.750	(14.683	101.8)[a]	13.695	2.670
			(14.607	133.4)[d]		
			14.266[b]			
Cu_5Sn_4 -η_1 (mP36)	44.44	328.971	(18.220	81.7)[a]	9.413	2.388
			18.282	81.7)[e]		
			17.309[f]			
Cu_5Sn_4 -η_2 (mC54)	44.44	328.620	(18.239	81.1)[a]	9.403	2.388
			(18.323	81.5)[e]		
			17.303[f]	84.6[g]		
Cu_6Sn_5 -η (mC44)	45.45	329.057	(18.428	80.9)[a]	9.223	2.374
			(18.512	79.6)[e]		
			17.777[f]	84.4[g]		
Ideal						
Cu_2Sn (hP6)	33.3	315.368	(16.366	87.9)[a]	11.512	2.540
			(16.352	88.0)[e]		
CuSn (hP4)	50	329.061	(19.335	75.1)[a]	8.432	2.319
			(19.350	76.5)[e]		
$CuSn_2$ (hP6)	66.7	304.334	(23.413	50.2)[a]	5.880	2.144
			(23.406	49.4)[e]		
Hypothetical						
Cu_3Sn (hP8)	25	331.900	14.628	106.8	13.747	2.670
Cu_7Sn_3 (aP40)	30	327.904	15.622		12.385	2.590
$Cu_{10}Sn_7$ (mC68)	41	323.132	17.628		10.011	2.432
$Cu_{11}Sn_9$ (mC20)	45	320.551	18.39		9.280	2.380
$CuSn_2$ (tI12)	66.7	317.460	21.566		6.384	2.144

[a] *Ab initio* PAW GGA calculations [4].
[b] Experimental data [44].
[c] *Ab initio* calculations [48].
[d] *Ab initio* calculations [49].
[e] *Ab initio* US-PP GGA calculations [50].
[f] Experimental data [16].
[g] Experimental data [50].

connection with the problem of relative stability of the stable IPs and the prediction of phase diagrams of multicomponent systems usually treated by the CALPHAD (*i.e.*, "Calculation of Phase Diagrams") method [1]. Within this method, the modeling of IPs using sublattice models within the Compound Energy Formalism (CEF), usually requires thermodynamic data of non-stable, hypothetical phases, for which *ab initio* methods can be of great value.

Also, there is a need for methods to systematize and interpret in microscopic terms the information provided by experiments, by phenomenological or empirical methods such as that developed by Miedema and collaborators [2,3], while obtaining reliable predictions of quantities which are poorly known from experiments or correspond to non-stable structures.

The general purpose of the present work is to present and analyze a theoretical database with the mentioned characteristics for a specific class of materials. Previous works by the current authors have been devoted to the theoretical calculation of the thermodynamic properties and the energy of formation (EOF) of various binary IPs occurring in systems usually considered as candidates for LFS applications, *viz.*, the Cu–In and Cu–Sn compounds of the Cu–In–Sn system [4], and the Ni–In and Ni–Sn compounds of the Ni–In–Sn system [5].

In these previous studies, detailed comparisons were presented

Table 4
Calculated cohesive energy, equilibrium atomic volume and bulk modulus for stable, metastable, ideal and hypothetical Ni–In intermetallic phases. The cohesive energy is given in kJ/mol-atom, the equilibrium volume (V_0) in Å^3/atom and the bulk modulus (B_0) in GPa. The valence electron density (n_{VED}) and the electron density at the boundary of the Wigner–Seitz cell (n_{WS}) are given in units of 4.6 10^{22} electrons cm^{-3}, following Miedema's approach.

Phase	at% In	E_{coh}	V_0	B_0	n_{VED}	n_{WS}
Stable						
Ni_3In (hP8)	25	437.589	(13.188	149.6)[a]	13.599	4.283
			(13.128	148.9)[b]		
			(13.154	156.0)[c]		
			13.031[d]			
Ni_3In (cP4)	25	435.339	(13.152	151.1)[a]	13.636	4.283
			(13.107	152.4)[b]		
			13.184[d]			
Ni_7In_3 (aP40)	30	426.723	(13.826	138.3)[a]	12.421	4.055
			13.606[e]			
Ni_2In (hP6)	33.33	412.307	(14.158	143.6)[a]	11.772	3.897
			(14.183	135.9)[b]		
			13.556[d]			
Ni_5In_3 (mC32)	37.5	409.859	(14.793	124.3)[a]	10.838	3.695
$Ni_{13}In_9$ (mC44)	40.9	401.256	(15.078	131.4)[a]	10.289	3.530
			14.400[d]			
NiIn (hP6)	50	384.792	(17.635	99.5)[a]	8.013	3.102
			(17.571	107.0)[b]		
			(17.683	102.0)[f]		
			(17.267	153.0)[g]		
Ni_2In_3 (hP5)	60	355.758	(18.278	94.5)[a]	6.898	2.681
			(18.277	93.2)[b]		
			17.358[d]			
Ni_3In_7 (cI40)	70	326.732	(20.090	77.1)[a]	5.519	2.326
			19.340[d]			
Hypothetical						
Ni_3In_2 (oP20)	40	404.890	15.482		10.110	3.574
NiIn (hP4)	50	371.338	(17.942	95.2)[h]	7.876	3.102
NiIn (hP4)	50	336.034	(21.734	64.3)[i]	6.501	3.102
Ni_3In_4 (mC14)	57	358.192	18.553		7.030	2.800
$NiIn_4$ (oC20)	80	290.855	23.392		4.089	2.037

[a] *Ab initio* PAW GGA calculations [5].
[b] FP-LAPW GGA-PBE [38].
[c] FP-LAPW GGA-PBE calculations (without relaxations of internal coordinates) [51,52].
[d] Experimental data [44].
[e] Experimental data [53,54].
[f] PAW GGA-PW91 [55].
[g] Experimental data [55].
[h] *Ab initio* PAW GGA calculations [6]; NiIn (hP6) with Ni vacancies on sites 2d.
[i] *Ab initio* PAW GGA calculations [6]; NiIn (hP6) with Ni vacancies on sites 2a.

Table 5
Calculated cohesive energy, equilibrium atomic volume and bulk modulus for stable, metastable, ideal and hypothetical Ni–Sn intermetallic phases. The cohesive energy is given in kJ/mol-atom, the equilibrium volume (V_0) in Å^3/atom and the bulk modulus (B_0) in GPa. The valence electron density (n_{VED}) and the electron density at the boundary of the Wigner–Seitz cell (n_{WS}) are given in units of 4.6 10^{22} electrons cm^{-3}, following Miedema's approach.

Phase	at% In	E_{coh}	V_0	B_0	n_{VED}	n_{WS}
Stable						
Ni_3Sn (hP8)	25	468.121	(13.021	166.7)[a]	14.191	4.126
			(13.106	162.0)[b]		
			12.890[c]			
Ni_3Sn (cF16)	25	463.817	(13.086	162.0)[a]	14.121	4.126
			(13.179	161.2)[b]		
			13.379[d]			
Ni_3Sn_2 (oP20)	40	448.457	(15.381	132.1)[a]	10.742	3.502
			(15.473	128.1)[b]		
			15.091[e]			
Ni_3Sn_4 (mC14)	57	413.737	(18.304	101.8)[a]	7.805	2.888
			(18.460	96.7)[b]		
			18.104[d]			
Metastable						
Ni_3Sn (cP4)	25	468.173	(13.030	163.6)[a]	14.181	4.126
			(13.120	163.4)[b]		
			13.057[d]			
$NiSn_4$ (oC20)	80	358.961	(23.433	57.5)[a]	4.824	2.273
			(23.558	55.5)[b]		
			23.392[f]			
Hypothetical						
Ni_2Sn (hP6)	33.33	450.606	14.115		12.321	3.773
Ni_7Sn_3 (aP40)	37.5	449.107	14.117		12.627	3.602
$Ni_{13}Sn_9$ (mC44)	40.9	441.295	15.090		10.870	3.467
NiSn (hp6)	50	426.385	17.612		8.640	3.125
NiSn (hP4)	50	429.943	(17.514	114.0)[g]	8.689	3.125
NiSn (hP4)	50	395.500	(21.374	73.8)[h]	7.120	3.125
Ni_2Sn_3 (hP5)	60	392.962	19.486		7.140	2.794
Ni_3Sn_7 (cI40)	70	374.571	21.057		5.988	2.511

[a] *Ab initio* PAW GGA calculations [5].
[b] *Ab initio* US-PP GGA calculations [37].
[c] Experimental data [56].
[d] Experimental data [44].
[e] Experimental data [25].
[f] Experimental data [26].
[g] *Ab initio* PAW GGA calculations [6]; NiSn (hP6) with Ni vacancies on sites 2d.
[h] *Ab initio* PAW GGA calculations [6]; NiSn (hP6) with Ni vacancies on sites 2a.

between the theoretical values and experimental data as well as other indirect information. In view of the satisfactory agreement shown by those comparisons, it seems appropriate to go on one step further and focus on the relations between cohesive properties, electronic structure and chemical bonding effects. Specifically, in the present work we rely upon the total-energy *versus* volume values determined in our previous studies [4–6] by *ab initio* projected augmented waves (PAW) calculations [7,8] using the VASP code [9], to determine the cohesive energy of Me–X phases (Me=Cu, Ni and X=In, Sn). We also treat several hypothetical IPs, involved in the use of the CEF to model the Gibbs energy of non-stoichiometric phases [1].

These present results are used to establish, for the first time, the systematic effects upon the cohesive energy, bulk modulus and volume of replacing Cu by Ni in a key group of compounds of interest in relation with the design of LFS alloys. Moreover, we establish new correlations between the cohesive properties of the Me–X phases (Me=Cu, Ni and X=In, Sn) and a single parameter describing the valence electron density. These correlations should be useful in the assessment of the available data and the estimation of unknown quantities, *e.g.*, the properties of non-stable structures. For the present purpose we consider all the phases and structures studied previously [4,5] which involve all the stable and metastable IPs of the accepted phase diagrams of the Cu–In [10–13], Cu–Sn [14–19], Ni–In [20,21] and Ni–Sn [22–27] systems.

Finally, using the electronic density of states also calculated in the present work, we develop a microscopic interpretation of the trends in cohesive properties for this family of IPs. The possibilities of a study of this type were highlighted by Gelatt, Williams and Moruzzi in a pioneering work on compounds formed by a transition metal and a non-transition element [28], by Freeman and coworkers on IPs with Al [29–31] and by other authors [32]. In the present work we show, in particular, how the systematics of cohesive properties can be understood in terms of a theoretical picture of the underlying bonding trends in the present class of materials.

2. Theoretical method

The total-energy values relied upon in the present work were obtained by spin polarized total energy DFT calculations, performed using the PAW method [7,8] and the VASP code [9].

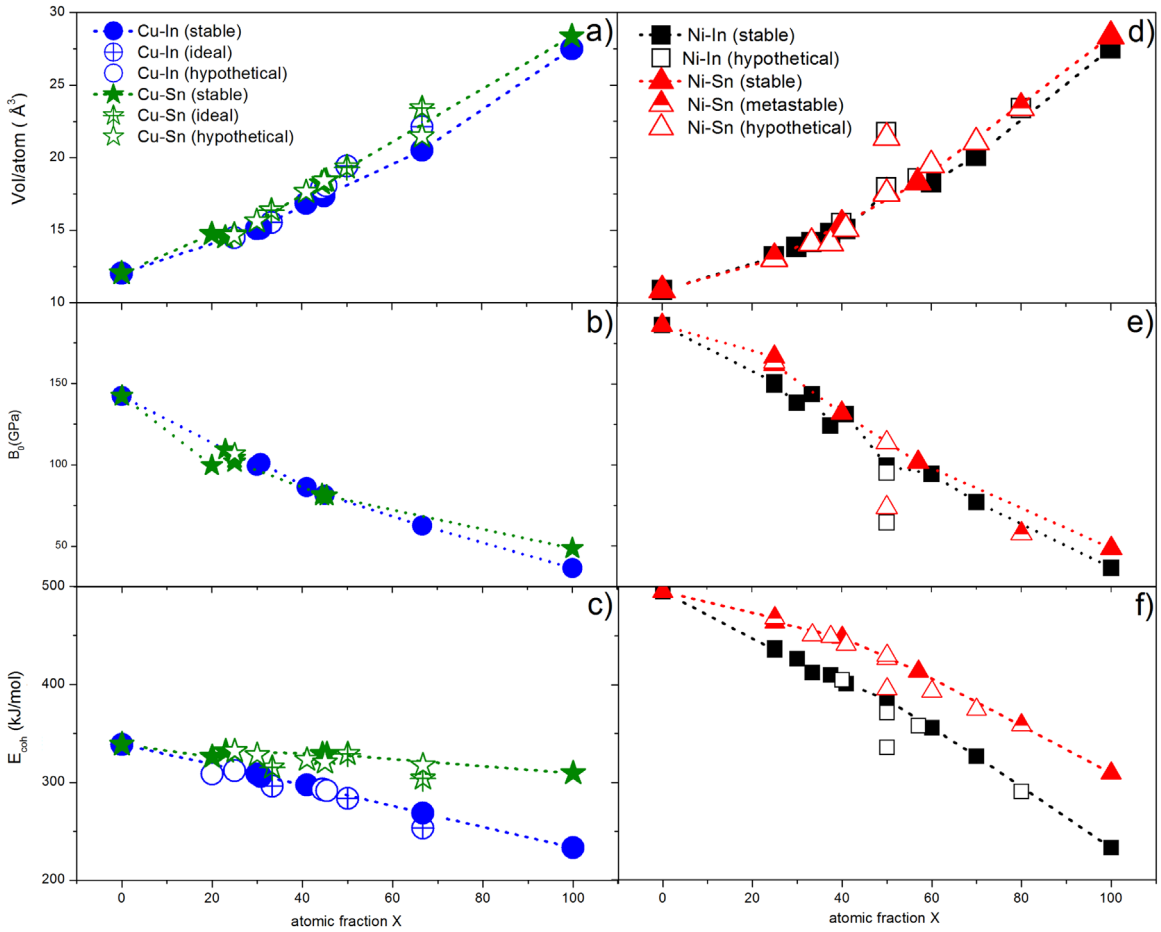

Fig. 1. Volume per atom (V_0), bulk modulus (B_0) and cohesive energy (E_{coh}) for stable, metastable, ideal and hypothetical Cu–In and Cu–Sn (1(a), 1(b) and 1(c)) and Ni–In and Ni–Sn (1(d), 1(e) and 1(f)) intermetallic phases, as functions of the atomic fraction of X (=In, Sn). Filled symbols refer to stable phases, half-filled symbols to metastable phases and empty symbols to non-stable phases (ideal and hypothetical).

Detailed accounts of the calculation method have been given elsewhere [4,5]. In the following we summarize only the points of relevance for the present study.

For the exchange-correlation energy we adopted the generalized gradient approximation due to Perdew and Wang (GGA-PW91) [33]. We considered 11 valence electrons for Cu ($3d^{10}4s^1$), 10 valence electrons for Ni ($3d^84s^2$), 3 for In ($5s^2p^1$) and 4 for Sn ($5s^2p^2$). The maximum kinetic energy for the expansion of plane waves was 314 eV for the Cu–X compounds and 330 eV for Ni–X compounds, X=In, Sn. The choice of the cutoff energy was tested until the changes in the total energies and in the cohesive energies were less than 10 meV/atom and 2 meV/atom, respectively.

The Brillouin zone integration was mapped on well-converged (within 1 meV/atom) Monkhorst–Pack k-point meshes [34] and the Methfessel–Paxton technique [35] with a smearing factor of 0.1 for the electronic levels. The criterion for the self-consistent convergence of the total energy was 0.1 meV. The unit cell and ionic degrees of freedom were optimized until Hellman–Feynman forces on the ions were lower than 30 meV/Å and the energy variations due to changes in the structural degrees of freedom were lower than 1 meV/atom.

To calculate the cohesive energy (E_{coh}) per atom of the Me_aX_b compound (Me=Cu, Ni and X=In, Sn), we followed the usual procedure [6,36], which requires additionally, the calculation of the total energies of the isolated Me=Cu,Ni and X=Sn,In atoms. For the present study we considered the stable, metastable and hypothetical IPs described in our previous studies for the Cu–In and Cu–Sn [4], Ni–In and Ni–Sn [5] systems. The various phases studied in the present work, 56 in total, are listed in Tables 2 to 5.

3. Ab initio database and systematics of cohesive properties

3.1. Calculated properties

In Table 1 we list the values of cohesive energy (E_{coh}), valence electron density (n_{VED}) and electron density at the boundary of the Wigner–Seitz cell (n_{WS}) of the elements Cu, Ni, In and Sn in their known equilibrium structures obtained in the present study. The electron density parameters will be defined latter in this section. In addition, and only as an aid in the discussions of trends, we also include in the Table the volume per atom (V_0) and bulk modulus (B_0) values for these elements, presented and compared elsewhere [4,5] with the available experimental data. It has been shown in those previous works that the present results for the equilibrium volume and bulk modulus compare very well with the available experimental data and with other *ab initio* calculations. Such an agreement adds to the confidence of the present theoretical technique. The cohesive energies show the typical DFT over-binding effect.

The full thermophysical database with new results for the Cu–In, Cu–Sn, Ni–In and Ni–Sn IPs is presented in Tables 2–5. There we list the calculated E_{coh}, reported here for the first time, the n_{VED} and n_{WS} for all the Cu–In, Cu–Sn, Ni–In and Ni–Sn IPs considered. These include stable, metastable and non-stable (*i.e.*, "hypothetical") compounds involved in CALPHAD-type modeling work of

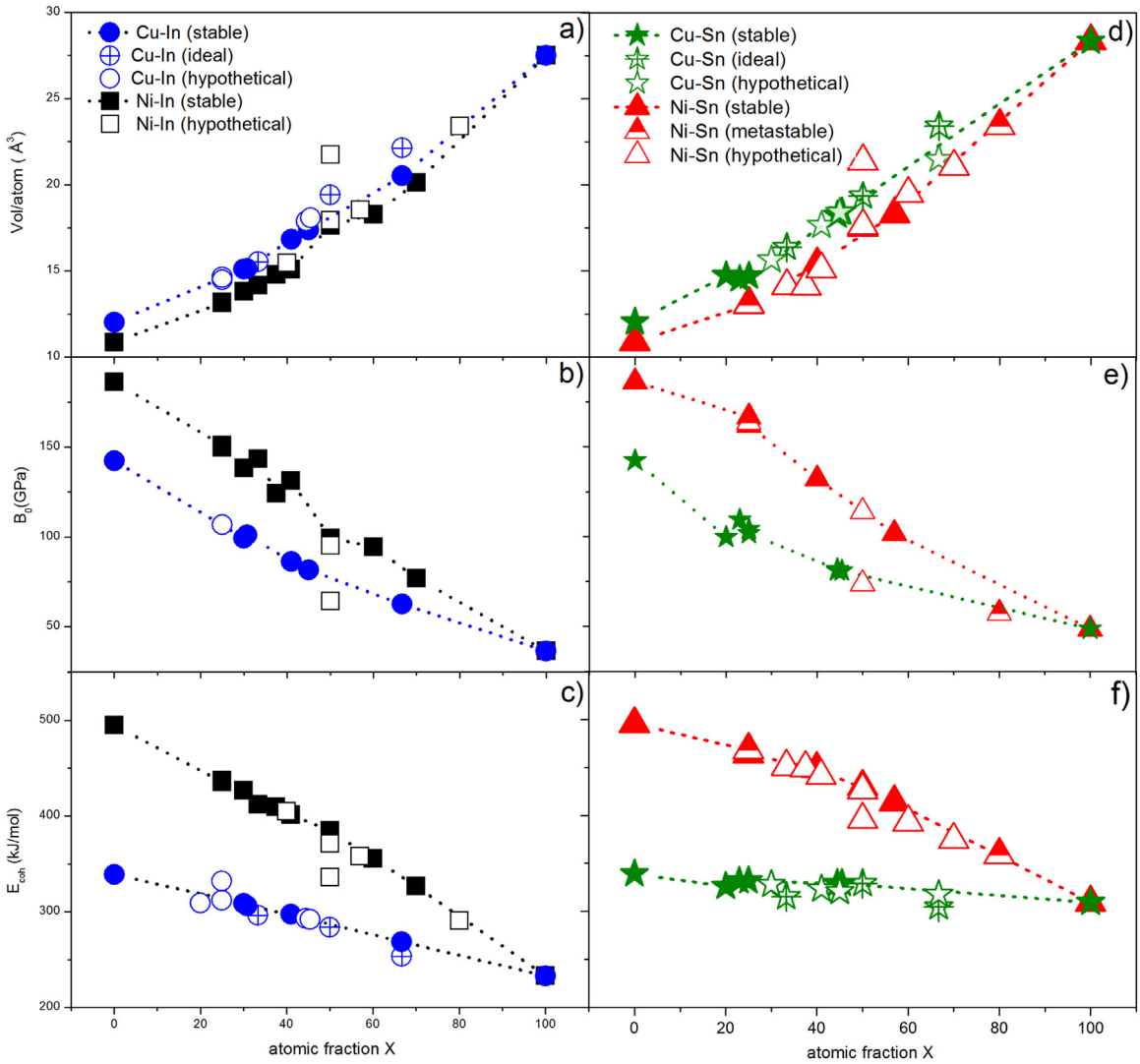

Fig. 2. Volume per atom (V_0), bulk modulus (B_0) and cohesive energy (E_{coh}) for stable, metastable, ideal and hypothetical Cu–In and Ni–In ((a), (b) and (c)) and Cu–Sn and Ni–Sn ((d), (e) and (f)) intermetallic phases, as functions of the atomic fraction of X (=In, Sn). Filled symbols refer to stable phases, half-filled symbols to metastable phases and empty symbols to non-stable phases (ideal and hypothetical).

these type of systems. We also include in these Tables the V_0 and B_0 values for these compounds, presented and compared elsewhere [4–6] with the available experimental data. In the following section we establish and analyze the composition and volume dependence of the remaining cohesive properties.

3.2. Composition dependence

The composition dependence of the calculated volume per atom (V_o), bulk modulus (B_0) and cohesive energy (E_{coh}) of the Cu–In and Cu–Sn IPs are compared in Fig. 1(a), (b) and (c), respectively. The corresponding comparisons for the Ni–In and Ni–Sn IPs are presented in Fig. 1(d), (e) and (f). According to Fig. 1, V_0 and B_0 of the Cu–In and Cu–Sn IPs show very close values. A similar trend is shown by V_0 and by B_0 of the Ni–In and Ni–Sn IPs. These results suggest that V_0 and B_0 of the Cu–X or the Ni–X (X=In,Sn) compounds mainly depends upon the content of the X element, and that the substitution of In by Sn in a given Me–X group of IPs (Me=Cu,Ni) does not influence significantly the values of these properties. On the other hand, this substitution does affect E_{coh}. In fact, Fig. 1(c) and (f), indicate that in both the Cu–X and the Ni–X group of compounds, E_{coh} for X=Sn is larger than for X=In.

The effects of substituting Cu by Ni in each group of Me–X compounds are studied in Fig. 2. According to Fig. 2(a) V_0 of the Me–In compounds decreases when changing Me=Cu by Me=Ni. Fig. 2(b) and (c) indicates that such a decrease is associated, respectively, with an increase in B_0 and E_{coh}, as generally expected. A similar trend is shown by Fig. 2(d), (e) and (f), *viz.*, V_0 of the Me–Sn compounds decreases, and B_0 and E_{coh} increases when changing Me=Cu by Me=Ni.

3.3. Volume dependence

The volume dependence of B_0 and E_{coh} for the Me–X compounds is studied in Fig. 3. B_0 of the Cu–X (X=In,Sn) compounds decreases with the increase in V_0, and the B_0 *vs.* V_0 relation corresponding to X=In, is very similar to that for X=Sn (Fig. 3(a)). Analogous trends are shown by the Ni–X compounds (Fig. 3(c)). These results suggest that in both, the Cu–X group and the Ni–X group (X=In,Sn) B_0 is mainly determined by V_0 of the compounds.

The variation of E_{coh} with V_0 shows some similarities and differences. As expected, E_{coh} for both the Cu–X (Fig. 3(b)) and Ni–X (Fig. 3(d)) groups (X=In,Sn) decreases with the increase in V_0. However, in each of these groups E_{coh} also depends upon the X element; specifically, for a given V_0, E_{coh} of the Cu–X and of the Ni–X compounds increases when changing X=In by X=Sn, as already

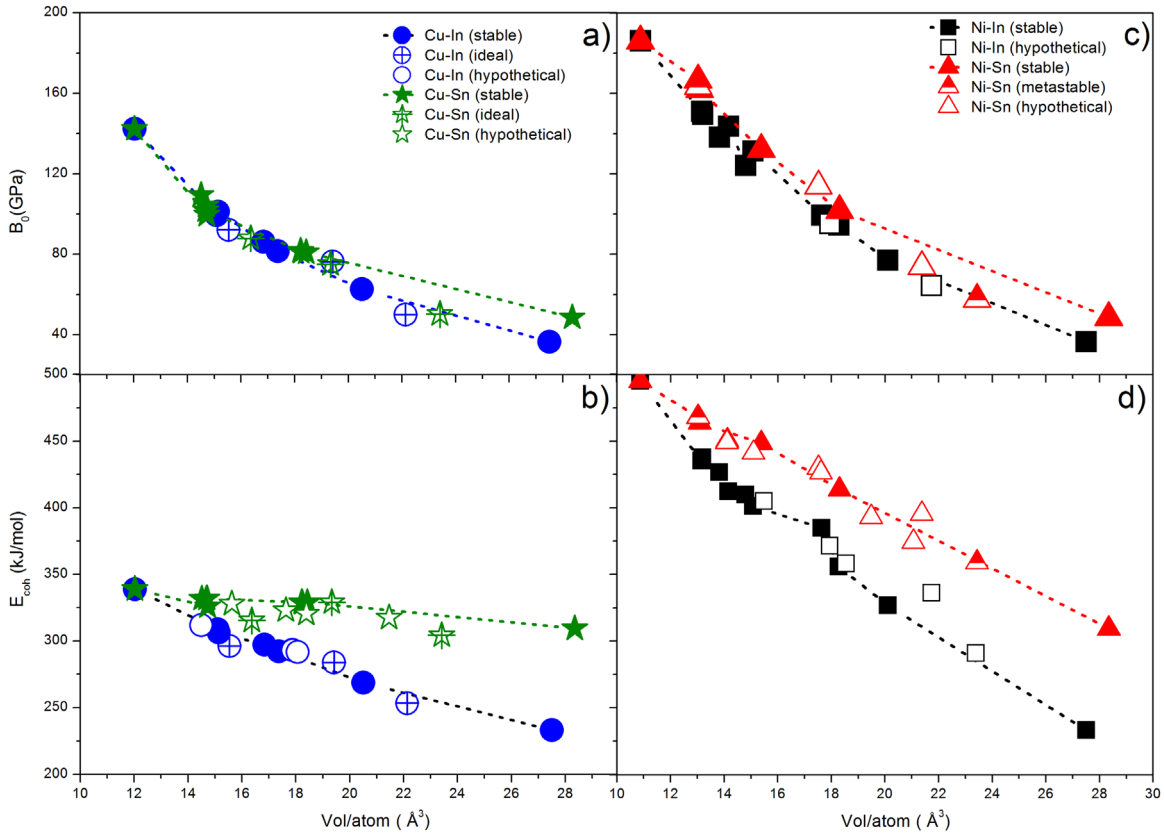

Fig. 3. Bulk modulus (B_0) and cohesive energy (E_{coh}) for stable, metastable, ideal and hypothetical Cu–In and Cu–Sn ((a) and (b)) and Ni–In and Ni–Sn ((c) and (d)) intermetallic phases, as functions of the volume per atom (V_0). Filled symbols refer to stable phases, half-filled symbols to metastable phases and empty symbols to non-stable phases (ideal and hypothetical).

found when discussing Fig. 1.

4. Electron-density correlations for cohesive properties

In the remainder of the present paper we will analyze the present results by adopting two complementary strategies. First, we will show in the present Section that the systematics of B_0 and E_{coh} established in the preceding one can be described in terms of a single parameter related to the density of valence electrons. Next, we will develop (Section 5) a microscopic interpretation of the bonding trends in the Me–X phases (Me=Cu, Ni and X= In, Sn).

4.1. Background

The use of variables related to the electronic density to systematize and predict cohesive properties of elements and compounds is an issue of long-standing empirical and theoretical interest in solid-state and materials science. A semi-empirical approach was presented long ago by Miedema, de Boer and de Chatel [57]. They suggested that a key contribution to the energetics of binary metallic alloys originates in the difference between the electron densities at the boundary of the Wigner–Seitz cell (n_{WS}) of the pure elements. Since no direct experimental information was available on n_{WS} they adopted an empirical approach based on combining: (i) theoretical band-structure results for Cu, Fe and Al, with (ii) estimates for Li, Na, K, Rb and Cs, based on assuming that in these metals the conduction electrons have an approximately uniform density throughout the atomic cell. Furthermore, Miedema et al. [2,3] established that these n_{WS} values correlated linearly with the experimental quantity $(B_0/V_0)^{1/2}$, and relied upon such correlation to estimate n_{WS} for transition metals and other elements. The so obtained n_{WS} for the elements were empirically adjusted in later works in order to improve the agreement with thermodynamic data on alloys [58]. Very recently, Li, Wu and collaborators proposed an empirical interpolation method to calculate n_{WS} for multicomponent IPs and showed that the resulting values also correlate linearly with the available $(B_0/V_0)^{1/2}$ of a large class of binary [59] and ternary [60] intermetallic alloys and compounds. Their interpolation method will be applied to calculate the n_{WS} of the present IPs, and the $(B_0/V_0)^{1/2}$ *vs.* n_{WS} plot based on the present results will be compared with an alternative representation, which was inspired on the following theoretical arguments.

Some theoretical insight on the microscopic origin of the Miedema correlations was presented in the pioneering study by Moruzzi et al. [61]. They showed that B_0 of the elements can be correlated with the interstitial charge density obtained in self-consistent band-structure calculations. Later on, the interstitial electron density (and the related bonding valence) was used by Rose, Shore and collaborators as a key parameter of a uniform electron gas model which accounts, in particular, for the trends in E_{coh} and B_0 of the transition, noble and simple metals [62]. Recently, Gilman et al. [63], showed that B_0 of the elements can, in fact, be correlated with the valence electron density (n_{VED}) given by the ratio between the number of valence electrons per atom and the atomic volume. The possibilities of this, remarkably simple approach, will be explored in the following.

4.2. New correlations for B_0 and E_{coh}

The key features of the present analysis are as follows: (i) following Gilman et al. [63] we use the parameter n_{VED}

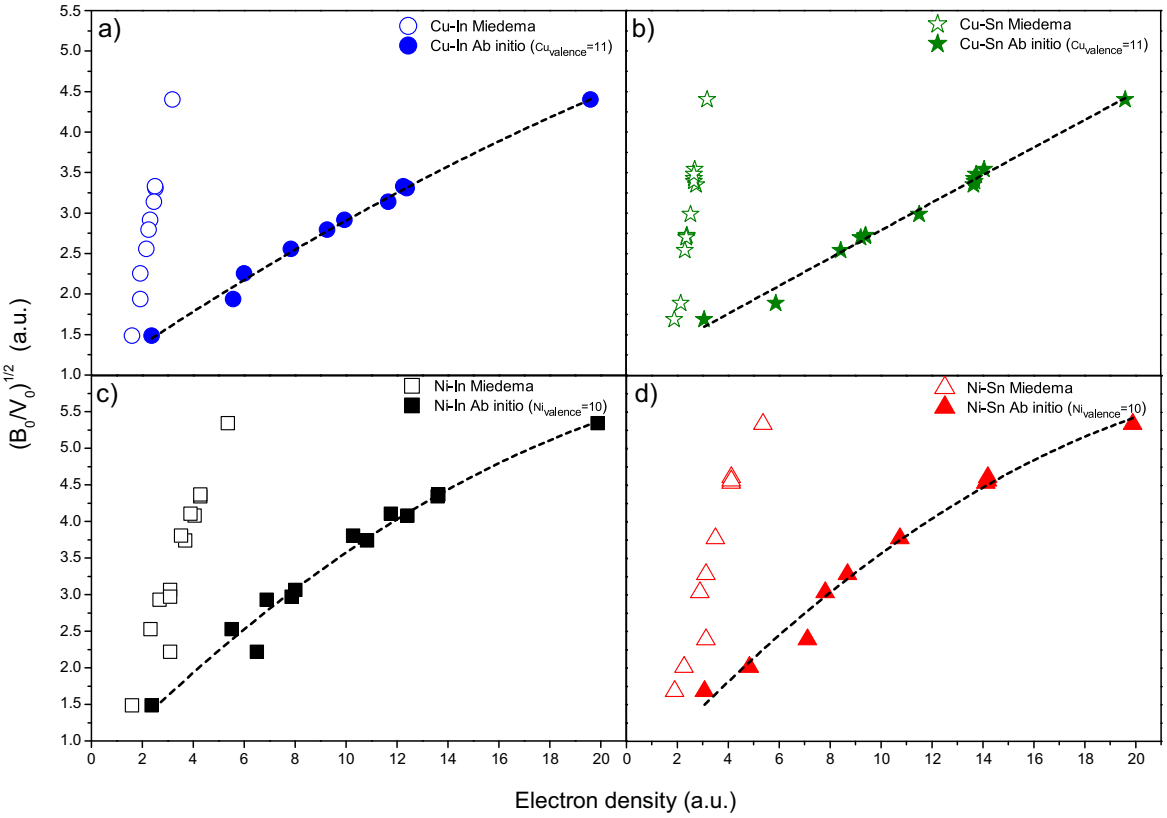

Fig. 4. Theoretical $(B_0/V_0)^{1/2}$ values for Cu–In (a), Cu–Sn (b), Ni–In (c) and Ni–Sn (d) intermetallics as functions of: (i) the Miedema parameter empirically related to the electron density at the boundary of the Wigner–Seitz cell (n_{WS}, empty symbols) calculated for the present IPs according to Ref. [42], and (ii) the valence electron density parameter (n_{VED}, filled symbols) defined in the present work. Both electron densities are expressed in units of 4.6 10^{22} electrons cm^{-3}. The plotted values of the quantity $(B_0/V_0)^{½}$ are expressed in arbitrary units as $\{10^{-6}$ [GPa]/[m^3 mol^{-1}]$\}^{1/2}$. The dashed lines are only guides to the eye.

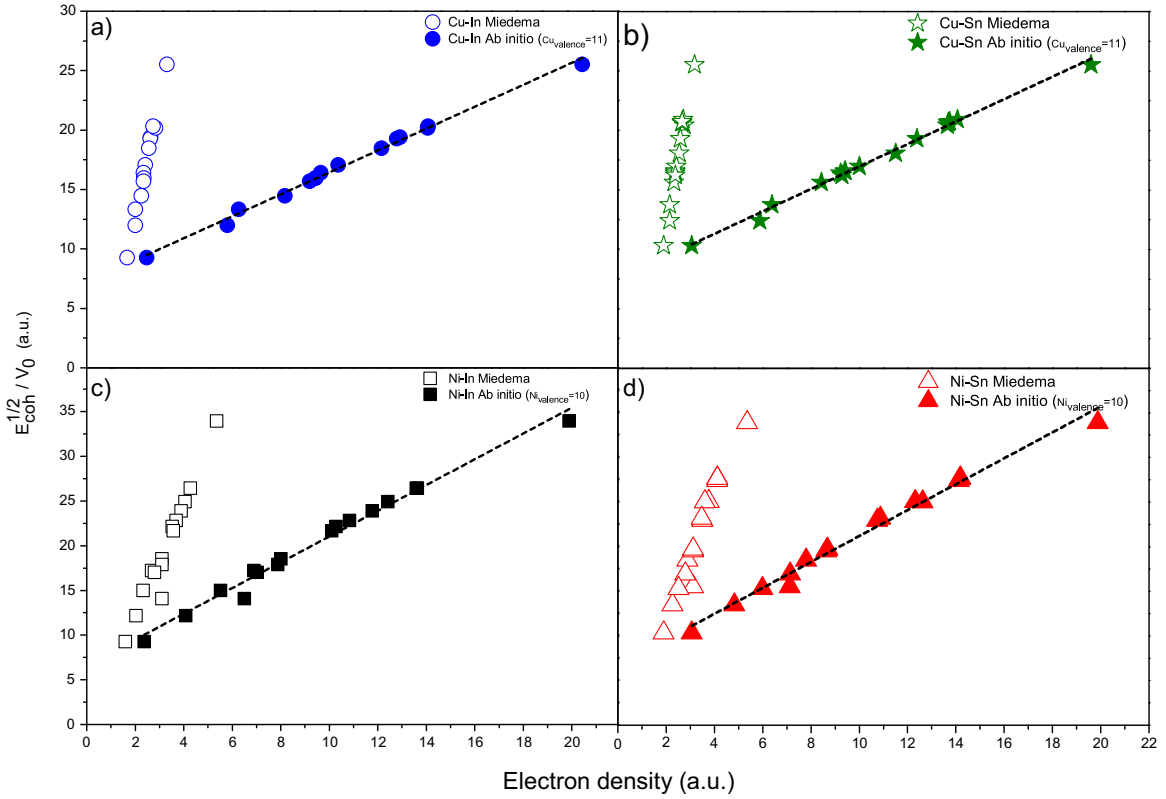

Fig. 5. Theoretical $[(E_{coh})^{1/2}/V_0]$ values for Cu–In (a), Cu–Sn (b), Ni–In (c) and Ni–Sn (d) intermetallics as functions of: (i) the Miedema parameter empirically related to the electron density at the boundary of the Wigner–Seitz cell (n_{WS}, empty symbols) calculated for the present IPs according to Ref. [42], and (ii) the valence electron density parameter (n_{VED}, filled symbols) defined in the present work. Both electron densities are expressed in units of 4.6 10^{22} electrons cm^{-3}. The plotted values of the quantity $[(E_{coh})^{1/2}/V_0]$ correspond to the following choice of units $([kJ\ mol^{-1}])^{1/2}/[m^3\ mol^{-1}]$. The dashed lines are only guides to the eye.

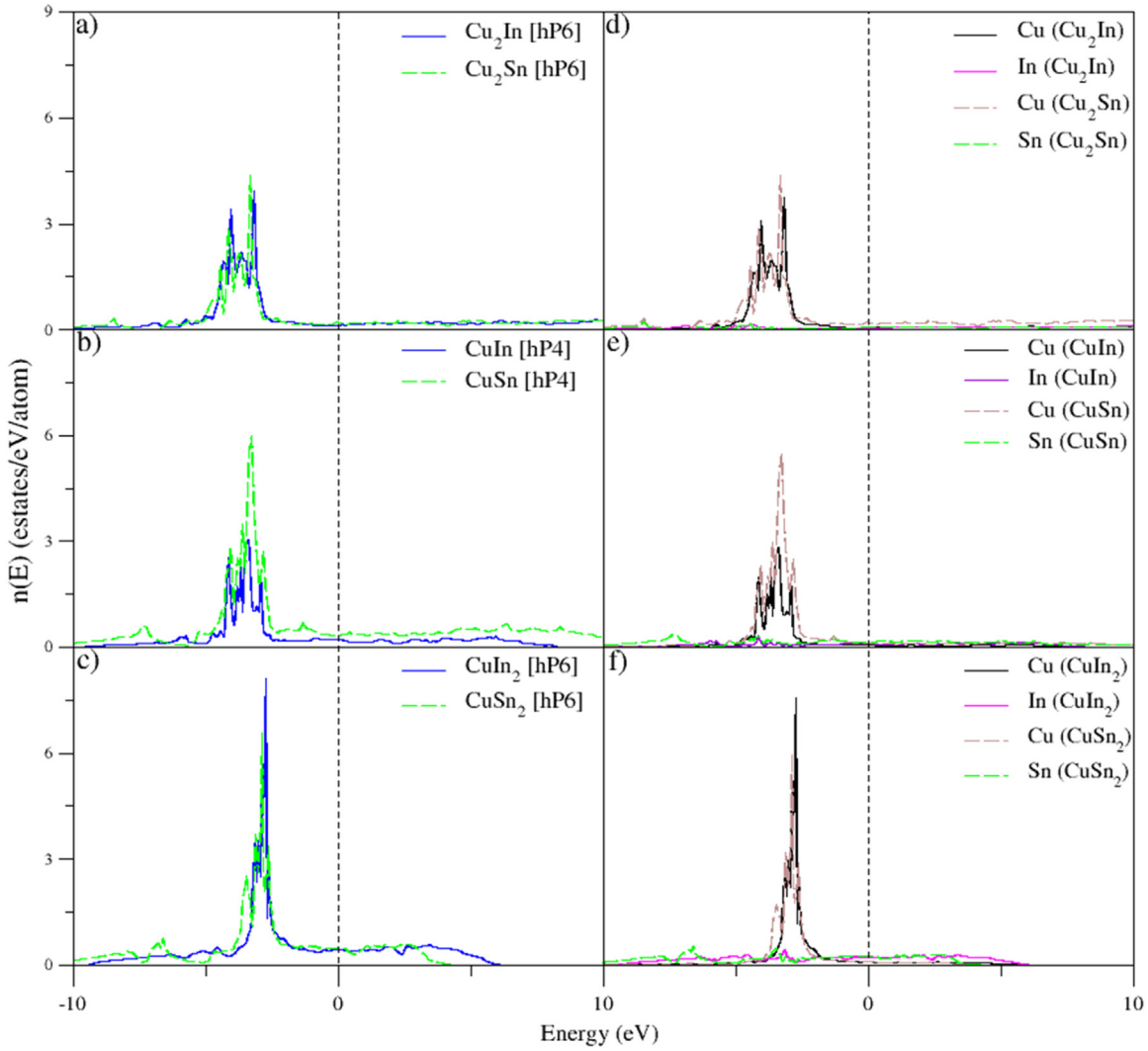

Fig. 6. Density of states (DOS) for (a) Cu_2X (hP6), (b) CuX (hP4) and (c) CuX_2 (hP6) structure compounds, with X=In (solid lines) and X=Sn (dashed lines). The atomic decomposed partial DOS are shown on the right panel (d–f). The origin of the scale corresponds to the Fermi level.

describing the number of valence electrons per unit volume; (ii) n_{VED} for the IPs is calculated by assuming for the elements the same number of valence electrons considered in our PAW calculations (*viz.* 11 valence electrons for Cu, 10 for Ni, 3 for In and 4 for Sn); (iii) in addition to stable phases, the results for metastable and non-stable (*i.e.*, ideal or hypothetical) ones are included; and, (iv) two correlations involving combinations of the quantities V_0, B_0, and E_{coh} and the n_{VED} parameter are established.

In Fig. 4 we plot the theoretical $(B_0/V_0)^{½}$ *vs.* n_{VED} values for the Cu–In (Fig. 4(a)), Cu–Sn (Fig. 4(b)) Ni–In (Fig. 4(c)) and Ni–Sn (Fig. 4(d)) intermetallics. The n_{VED} parameter is expressed in units of 4.6 10^{22} electrons cm^{-3}. In order to compare with the Miedema approach, the plotted values of the quantity $(B_0/V_0)^{½}$ are expressed in arbitrary units as $\{10^{-6}$ [GPa]/ $[m^3\ mol^{-1}]\}^{1/2}$. For comparisons we plot the same $(B_0/V_0)^{½}$ values *vs.* the n_{WS} obtained by applying to the Miedema values for the elements the interpolation method for alloys developed by Li and Wu [59]. These graphics demonstrate that: (i) a reasonably well defined correlation between $(B_0/V_0)^{½}$ and n_{VED} for the Cu–In, Cu–Sn, Ni–In and Ni–Sn intermetallics is found; (ii) the scatter of the $(B_0/V_0)^{½}$ *vs.* n_{VED} correlation is, in general, comparable to that of the $(B_0/V_0)^{½}$ *vs.* n_{WS} representation; (iii) the $(B_0/V_0)^{½}$ *vs.* n_{VED} relation deviates negatively from linearity when approaching Cu (Fig. 4(a) and (b)) and Ni (Fig. 4(c) and (d)).

It should be emphasized that in order to approach the correlation based on the Miedema parameters while keeping the theoretical V_0 and B_0 results, it would be necessary to assume for Cu and Ni n_{VED} values corresponding approximately to 2 and 3 valence electrons, respectively. These numbers are significantly smaller than those included in the PAWs, but comparable to the usual chemical valence of these elements [64].

The cohesive energy E_{coh} was not included in the correlations by Li and Wu [59] or by Li et al. [60]. However, guided by the covariation of cohesive properties demonstrated in Figs. 2 to 4, and noting that on purely dimensional grounds the $(B_0/V_0)^{½}$ quantity corresponds to the $(E_{coh}^{½}/V_0)$ ratio, we will study the effect of changes in n_{VED} upon the later quantity.

In Fig. 5 we plot *vs.* n_{VED} the theoretical $(E_{coh}^{½}/V_0)$ values for Cu–In (Fig. 5(a)), Cu–Sn (Fig. 5(b)), Ni–In (Fig. 5(c)) and Ni–Sn (Fig. 5(d)) compounds. The plotted values of the latter quantity correspond to the following choice of units $([kJ\ mol^{-1}])^{1/2}/[m^3\ mol^{-1}]$. These graphics demonstrate that remarkably well defined linear correlations can be established between the theoretical $(E_{coh}^{½}/V_0)$ values and the valence electron density parameter n_{VED}. Indeed, linear correlations can also be established between $(E_{coh}^{½}/V_0)$ and the n_{WS} parameter based on the Miedema approach. In view of the comparable accuracy of both correlations, it seems justified to conclude that the use of empirically generated n_{WS} parameters is, in fact, not necessary.

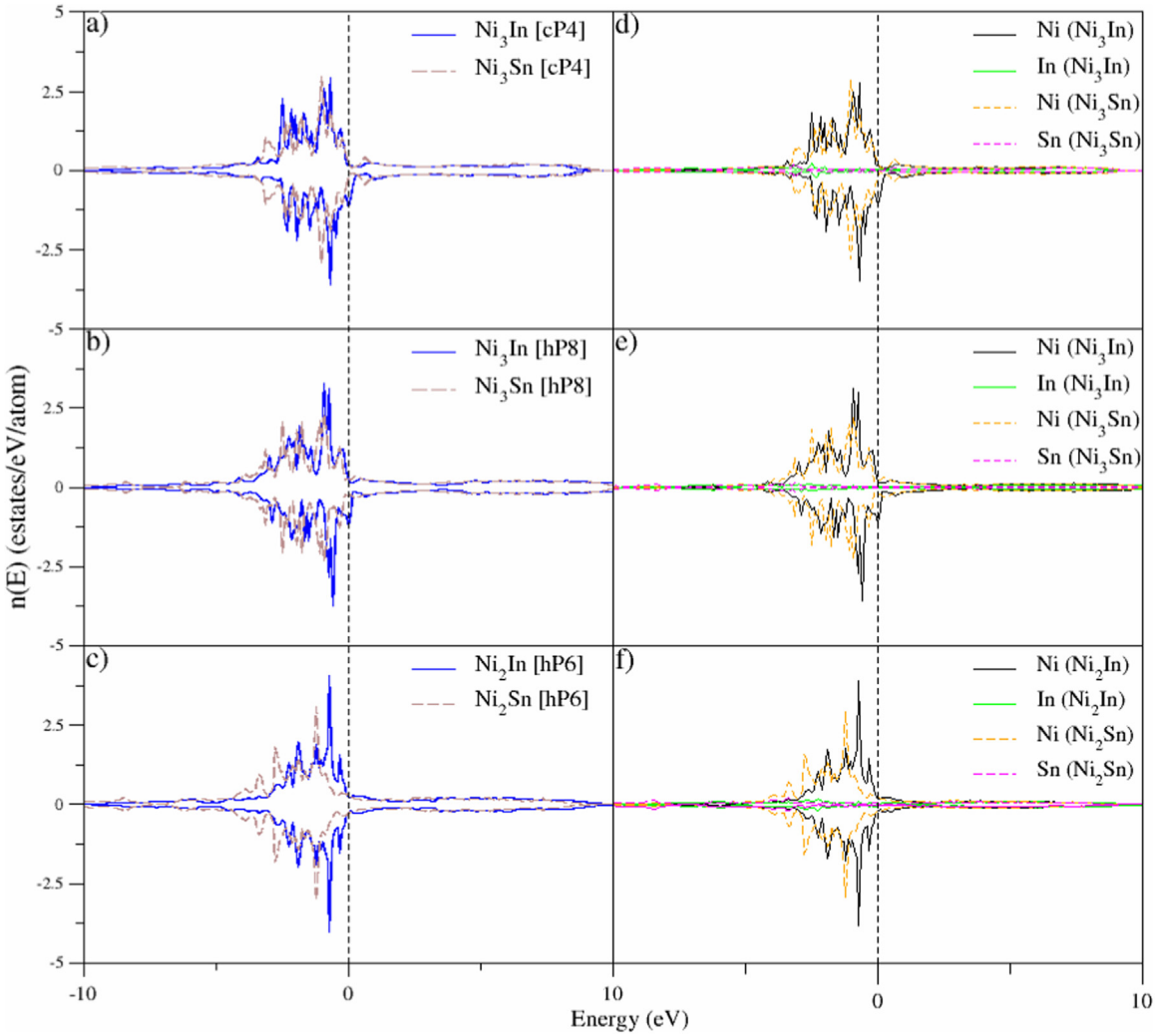

Fig. 7. Density of states (DOS) for a) Ni_3X (cP4), b) Ni_3X (hP8), c) Ni_2X (hP6) compounds, with X=In (solid lines) and X=Sn (dashed lines). The atomic decomposed partial DOS are shown on the right panel (d–f). The origin of the scale corresponds to the Fermi level. Positive (negative) values correspond to spin up (down) contributions.

5. Electronic structure and interpretation of bonding trends

5.1. General considerations

In view of the co-variation of cohesive properties suggested by the results of the previous section we will study the electronic structure and develop a microscopic interpretation of the key systematic features emerging from the comparisons in the previous section. To this end we will select a number of iso-structural compounds of Cu and Ni with In and Sn and compare the various contributions to the electronic density-of-states (DOS) and the chemical bonding. In such analysis we will rely mainly on the theory by Gelatt, Williams and Moruzzi [28]. Other studies of the relations between the DOS and the properties of the IPs will also be considered [29–31,65]. There are two main contributions to the electronic structure for this class of compounds [28]. One is the lattice expansion effect due to the insertion of an *sp* element in a transition metal lattice, and the second is the interaction between the valence *d* shell of the transition metal with the valence *sp* shell of the non-transition element (In or Sn for the presently studied compounds). The largest contribution to the cohesive energy comes from the formation of a *d* band from the atomic *d* transition metal orbitals. By the insertion of a *sp* element the lattice expands, and the *d* band-width decreases therefore reducing the stability of the lattice. The second ingredient in the electronic structure behavior is the covalent hybridization of the atomic states in which the *d* states of a transition metal hybridize with the *p* states of the non-transition element to form a bonding hybrid, more tightly bound than either of the states from which it originates. These two ingredients will be considered in the following analysis to establish correlations between the electronic structure and cohesive properties [28].

5.2. Comparisons of Me–In and Me–Sn compounds with Me=Cu,Ni

The results in Section 3 indicate that in each Me–X group of compounds (Me=Cu,Ni) E_{coh} decreases with the increase in the X content, while for a given X content, E_{coh} for the IPs with X=Sn is larger than when X=In. Seeking an electronic-structure explanation for these regularities we will perform two series of comparisons.

In the first place we will compare the DOS and E_{coh} of three pairs of Cu–X compounds based on the ideal Ni_2In–NiAs type structures, *viz.*, Cu_2X (hP6), CuX (hP4) and CuX_2 (hP6). The calculated DOS are presented in Fig. 6(a), (b) and (c), respectively. As discussed in previous works, the DOS are mainly determined by the Cu 3d electronic states, with minor contributions of 5*s* and 5*p* In or Sn orbitals with the bottom of their bands lying deeper in energy with respect to the Fermi level. The *s*-band appears at

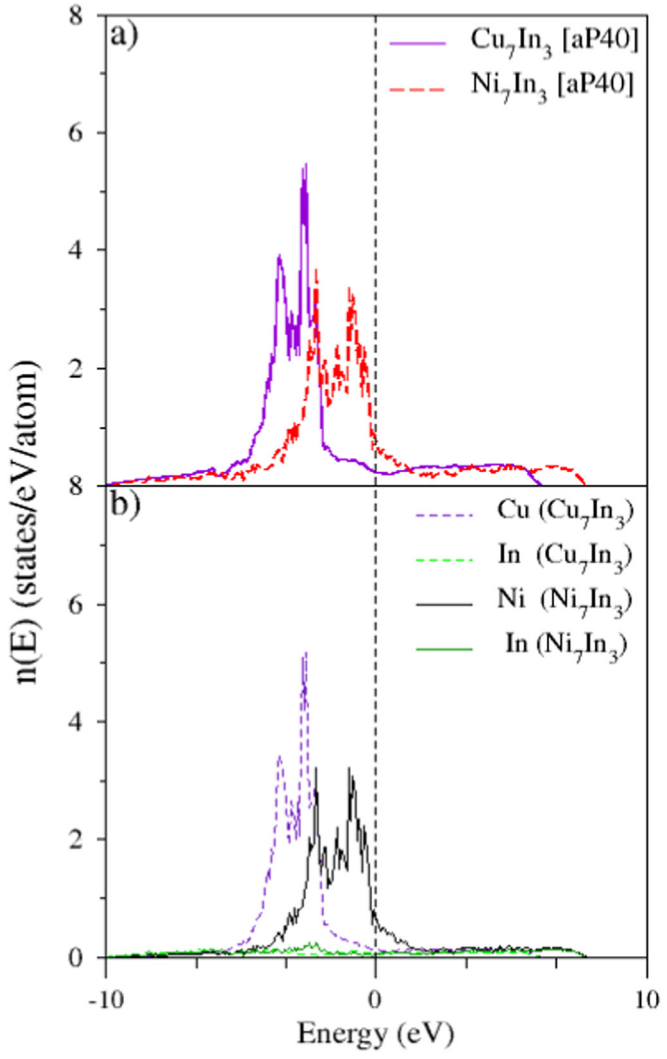

Fig. 8. (a) Density of states (DOS) for the Me_7In_3 (aP40) structure compounds with Me=Cu (solid lines) and Me=Ni (dashed lines); b) the atomic decomposed partial DOS. The origin of the scale corresponds to the Fermi level.

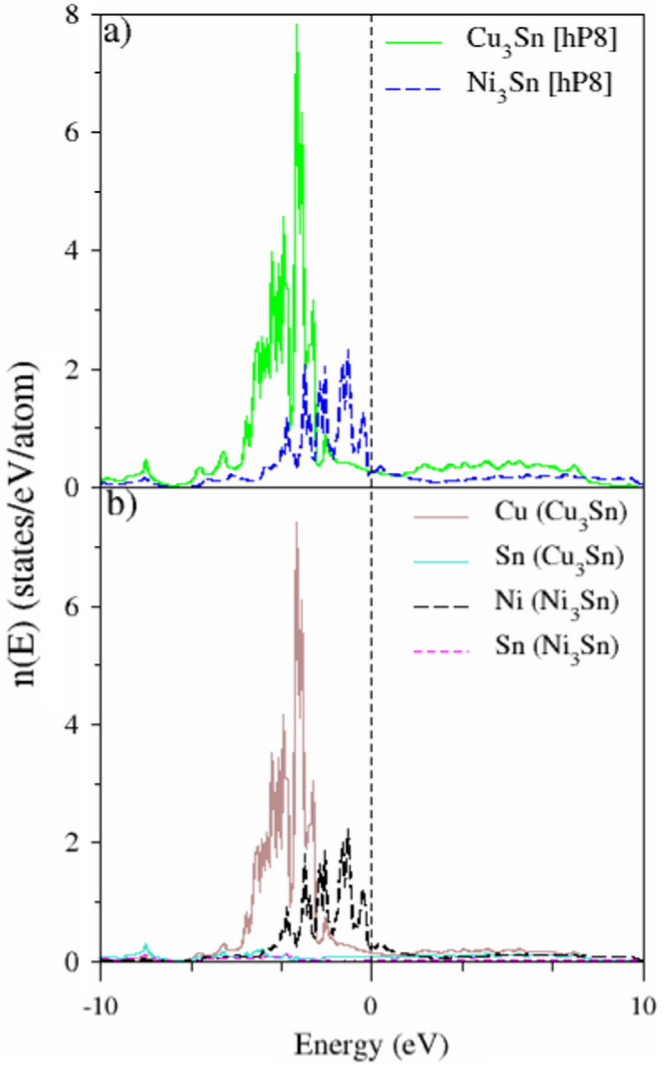

Fig. 9. (a) Density of states (DOS) for the Me_3Sn (hP8) structure compounds, with Me=Cu (solid lines) and Me=Ni (dashed lines); (b) the atomic decomposed partial DOS. The origin of the scale corresponds to the Fermi level.

lower energies and is clearly separated from the *p*-band, which extends to energies higher than the Fermi level. Another important feature of the DOS contributing to bonding in this type of compounds is the presence of hybridization effects between the Cu-3*d* electronic orbitals and 5*p*-electrons of In or Sn. Fig. 6 indicates that with the increase of the X-content in the compound, the main band in the DOS moves towards the Fermi energy and decreases its width. This band-narrowing effect can be correlated to the reduction in the number of Cu–Cu bonds and the increase in the atomic volume with increasing the X-content for these compounds (Fig. 1(a)). In addition, the separation between bonding and anti-bonding states, seemingly corresponding to the valley in the two-peak DOS structure of Cu_2X, gets more diffuse. The reduction of the *d* band-width also suggests, in turn, that the *d*-states in the compounds with the largest X content are less hybridized [66]. Both effects would lead to a decrease in the cohesion of the Cu–X compounds with the increase in the X content, as established in the present work. We also note that the width of the main band for each of the Sn compounds is slightly larger than that of the corresponding In compounds. This behavior correlates with the smaller atomic volume of the former ones (see Fig. 1(a)), and explains their higher cohesion.

In the second place, we will compare the DOS and E_{coh} of three pairs of Ni–X compounds with X=In,Sn, *viz.*, Ni_3X (cP4), Ni_3X (hP8) and Ni_2X (hP6). The calculated DOS are presented in Fig. 7 (a), (b) and (c), respectively. The main features discussed above for the DOS of the Cu–In and Cu–Sn compounds (Fig. 6) are observed, in general, for the Ni–In and Ni–Sn compounds (Fig. 7). One of the most important differences is, however, the fact that the main band lies closer to the Fermi level. Only the Ni_3In compound is ferromagnetic. For the three non-magnetic compounds (Ni_3Sn cP4 and hP8) and Ni_2In and Ni_2Sn (hP6) the Fermi level is located at a deep of the DOS, on the right border of the main bonding band. In all the structures and compounds considered in Fig. 7, the Ni–Sn compounds have smaller atomic volumes (see Tables), a fact that is reflected in the larger band-widths observed for Ni–Sn compounds; the stronger cohesion and bonding of these compounds can be related to this fact.

When comparing the relative stability of both, the cP4 and hP8 phases, one can see that the relatively more stable hP8 phase has a DOS whose band-width is larger, with electronic states extending to lower energies at the left side of the main band in the DOS.

5.3. Comparisons of Cu–X and Ni–X compounds with X=In,Sn

Another key result of Section 3 is that in each group of Me–X compounds (X=In,Sn) the substitution of Me=Cu by Me=Ni leads to an increase in E_{coh}. In order to provide an electronic-structure explanation for this regularity we will perform two series on comparisons.

In the first place, we choose the Me_7In_3 (aP40) structure and compare the DOS and E_{coh} of the compound with Me=Cu with that for the IP with Me=Ni. The calculated DOSs are presented in Fig. 8. We note that both DOSs are qualitatively similar in shape, and that the substitution of Cu by Ni leads to a shift of the DOS towards the Fermi energy. In both cases the expected anti-bonding states corresponding to the highest energy part of the DOS, are almost completely occupied in the Cu–In compounds, but partially and less occupied for the Ni compound.

In the second place, we choose the Me_3Sn (hP8) structure and compare the DOS and E_{coh} of the compound with Me=Cu with that for Me=Ni. The calculated DOS are presented in Fig. 9. This comparison suggests that the effects of substituting Cu by Ni in this structure are analogous to those observed in the Me_7In_3 (aP40) compounds.

6. Summary and concluding remarks

The theme of the present work is the use of systematic *ab initio* calculations to study the volume per atom (V_0), bulk modulus (B_0), cohesive energy (E_{coh}) and the electronic density of states (DOS) of a large group of Cu–In, Cu–Sn, Ni–In and Ni–Sn intermetallic phases (IPs). To this end, an extensive database with total-energy *versus* volume values progressively developed by the current authors-by means of projected augmented waves (PAW) calculations using the VASP code-is expanded by incorporating the cohesive energy and the electronic density of states.

The expanded database is used, in the first place, to establish trends in the composition dependence of V_0, the composition and volume dependence of B_0 and E_{coh} for several Me–X phases (Me=Cu,Ni, X=In,Sn) reported as stable and metastable, as well as various hypothetical compounds involved in the thermodynamic modeling of IPs using the Compound-Energy Formalism.

In the second place, the following systematic effects of relevance for the design of lead-free soldering alloys are highlighted for the first time: (i) V_0 and B_0 of the Cu–X or the Ni–X (X=In,Sn) IPs mainly depend upon the content of the X element; (ii) in each Me–X group of compounds (Me=Cu,Ni) E_{coh} is larger when X=Sn than for X=In; (iii) in both the Me–In and Me–Sn compounds V_0 decreases while B_0 and E_{coh} increases when changing Me=Cu for Me=Ni; and, (iv) in both the Cu–X and the Ni–X compounds (X=In,Sn) B_0 is mainly controlled by V_0.

Moreover, two correlations expressing the variation of the quantities $(B_0/V_0)^{1/2}$ and $(E_{coh}^{1/2}/V_0)$ with the valence electron density are demonstrated, and compared in detail with analogous correlations involving an empirical parameter related to the electron density at the boundary of the Wigner–Seitz cell proposed in the Miedema approach.

Finally, an analysis is performed of the DOS of various representative iso-structural Me–X compounds (Me=Cu,Ni, X=In, Sn) by considering the interaction between Cu or Ni *d*-electrons and In or Sn *s* and *p*-electrons. In this way, a microscopic interpretation is provided of the trends in cohesive properties established in the current work.

Acknowledgment

This work was supported by Project PIP 112-20110100814 from CONICET and Project I197 from Universidad Nacional del Comahue.

References

[1] M. Hillert, J. Alloy. Compd. 330 (2001) 161–176.
[2] A.R. Miedema, R. Boom, F.R. de Boer, J. Less-Common Met. 41 (1975) 283–289.
[3] A.R. Miedema, R. Boom, F.R. de Boer, J. Less-Common Met. 46 (1976) 67–83.
[4] S. Ramos de Debiaggi, C. Deluque Toro, G. Cabeza, A. Fernández Guillermet, J. Alloy. Compd. 542 (2012) 280–292.
[5] S. Ramos de Debiaggi, C. Deluque Toro, G.F. Cabeza, A. Fernández Guillermet, J. Alloy. Compd. 576 (2013) 302–316.
[6] S. Ramos de Debiaggi, N.V. González Lemus, C. Deluque Toro, A. Fernández Guillermet, J. Alloy. Compd. 619 (2015) 464–473.
[7] P.E. Blöchl, Phys. Rev. B 50 (1994) 17953–17979.
[8] G. Kresse, J. Joubert, Phys. Rev. B 59 (1999) 1758–1775.
[9] G. Kresse, J. Furthmüller, Comput. Mater. Sci. 6 (1996) 15–50.
[10] H. Okamoto, T.B. Massalski, J. Phase Equilib. 15 (1994) 500–521.
[11] W. Keppner, T. Klas, W. Körner, R. Wesche, G. Schatz, Phys. Rev. Lett. 54 (1985) 2371–2374.
[12] A. Bolcavage, S.W. Chen, C.R. Kao, Y.A. Chang, A.D. Roming Jr., J. Phase Equilib. 14 (1993) 14–21.
[13] S. Piao, S. Lidin, Z. Anorg. Allg. Chem. 634 (2008) 2589–2593.
[14] N. Saunders, A.P. Miodownik, J. Phase Equilib. 11 (1990) 278–287.
[15] W. Köster, T. Gödecke, D. Heine, Z. Metallkd. 63 (1972) 802–807.
[16] S. Lidin, A.K. Larsson, J. Solid State Chem. 118 (1995) 313–322.
[17] M. Elding-Pontén, L. Stenberg, S. Lidin, J. Alloy. Compd. 261 (1997) 162–171.
[18] A.K. Larsson, L. Stenberg, S. Lidin, Acta Crystallogr. B 50 (1994) 636–643.
[19] A.K. Larsson, L. Stenberg, S. Lidin, Z. Kristallogr. 210 (1995) 832–837.
[20] M.F. Singleton, P. Nash, Binary Alloy Phase Diagrams, T.B. Massalski, (Ed.), ASM, Metals Park, OH, 1990, vol. 3.
[21] Ph Durussel, G. Burri, P. Feschotte, J. Alloy. Compd. 257 (1997) 253–258.
[22] T.B. Massalski, H. Okamoto, P.R. Subramanian, L. Kacprak, Binary Alloy Phase Diagrams 2 ed, ., ASM, Materials Park, OH (1990), p. 2863.
[23] H.R. Pak, T. Saburi, S. Nenno, Bull. Jpn. Inst. Met 37 (1973) 1128–1134.
[24] A. Leineweber, M. Ellner, E.J. Mittermeijer, J. Solid State Chem. 159 (2001) 191–197.
[25] A. Leineweber, O. Oeckler, U. Zachwieja, J. Solid State Chem. 177 (2004) 936–945.
[26] W.J. Boettinger, M.D. Vaudin, M.E. Williams, L.A. Benderky, W.R. Wagner, J. Electron. Mater. 32 (2003) 511–515.
[27] T. Watanabe, K. Arai, T. Hirose, M. Chikazawa, J. Jpn. Inst. Met. 63 (1999) 496–501.
[28] C.D. Gelatt, A.R. Williams, V.L. Moruzzi, Phys. Rev. B 27 (1983) 2005–2013.
[29] T. Hong, T.J. Watson-Yang, X.Q. Guo, A.J. Freeman, T. Oguchi, J. Xu, Phys. Rev. B 43 (1991) 1940–1947.
[30] J. Xu, A.J. Freeman, Phys. Rev. B 40 (1989) 11927–11930.
[31] J. Xu, A.J. Freeman, Phys. Rev. B 41 (1990) 12553–12561.
[32] C. Colinet, A. Pasturel, P. Hicter, Calphad 9 (1985) 71–99.
[33] J.P. Perdew, Y. Wang, Phys. Rev. B 45 (1992) 13244–13249.
[34] H.J. Monkhorst, J.D. Pack, Phys. Rev. B 13 (1976) 5188–5192.
[35] M. Methfessel, A.T. Paxton, Phys. Rev. B 40 (1986) 3616–3621.
[36] R.A. Evarestov, Springer Science Business Media, 2007, 574.
[37] G. Ghosh, Metall. Mater. Trans. A 40 (2009) 4–23.
[38] C. Deluque Toro, S. Ramos de Debiaggi, A.M. Monti, Physica B 407 (2012) 3236–3239.
[39] G. Alers, J.R. Neighbours, H. Sato, J. Phys. Chem. Solids 13 (1960) 40–45.
[40] S. Ramos de Debiaggi, G.F. Cabeza, C. Deluque Toro, A.M. Monti, S. Sommadossi, A. Fernández Guillermet, J. Alloy. Compd. 509 (2011) 3238–3245.
[41] M.E. Straumanis, L.S. Yu, Acta Crystallogr. A 25A (1969) 676–682.
[42] M. Kantola, E. Tokola, Physics 223A (1967) 1–10.
[43] E.C. Overton, Jr.J. Gaffney, Phys. Rev. 98 (1955) 969–977.
[44] P. Villars, Pearson's, Handbook of Crystallographic Data for Intermetallic Phases, Desk Edition, ASM, Materials Park, OH (1997), p. 2189.
[45] K. Takemura, Phys. Rev. B 44 (1991) 545–549.
[46] J.A. Rayne, B.S. Chandrasekhar, Phys. Rev. 120 (1960) 1658–1663.
[47] C. Kittel, Introduction to Solid State Physics 6 ed., New York, John Wiley and Sons, 1986.
[48] R. An, Ch Wang, Y. Tian, H. Wu, J. Electron. Mater. 37 (2008) 477–482.
[49] J. Chen, Y. Lai, Ch Ren, D. Huamg, Appl. Phys. Lett. 92 (2008) 081901.
[50] G. Ghosh, M. Asta, J. Mater. Res. 20 (2005) 3102–3117.
[51] G.Y. Guo, Y.K. Wang, Li. Shing Hsu, J. Magn. Magn. Mater 239 (2002) 91–93.
[52] G.Y. Guo, Y.K. Wang, Li. Shing Hsu, Phys. Rev. B 66 (2002) 054440–054448.
[53] L. Norén, R.L. Withers, Y. Tabira, J. Alloy. Compd. 309 (2000) 179–187.
[54] L. Norén, A.K. Larsson, R.L. Withers, H. Rundlöf, J. Alloy. Compd. 424 (2006) 247–254.
[55] A.S. Mikhaylushkin, T. Sato, S. Carlson, S.I. Simak, U. Häussermann, Phys. Rev. B 77 (2008) 014102–014108.

[56] A.L. Lyubimtsev, A.L. Baranov, A. Fisher, L. Kloo, B.A. Popovkin, J. Alloy. Compd. 340 (2002) 167–172.
[57] A.R. Miedema, F.R. de Boer, P.F. de Chatel, J, **3** (1973).
[58] A.R. Miedema, Physica B 182 (1992) 1–17.
[59] C. Li, P. Wu, Chem. Mater. 13 (2001).
[60] C. Li, Y.L. Chin, P. Wu, Intermetallics 12 (2004) 103–109.
[61] V.L. Moruzzi, J.F. Janak and A.R. Williams, Pergamon Press Inc., 1978.
[62] M. Sigalas, J.H. Rose, D.A. Papaconstantopoulos, H.B. Shore, Phys. Rev. B 58 (1998) 13438–13441.
[63] J.J. Gilman, R.W. Cumberland, R.B. Kaner, Int. J. Refract. Met. Hard Mater. 24 (2006) 1–5.
[64] D.M. Adams, John Wiley & Sons, 1974, pp. 32–34.
[65] P. Ravidran, R. Asokamani, Bull. Mater. Sci. 20 (1997) 613–622.
[66] O. Granäs, P.A. Korzhavyi, A.E. Kissavos, I.A. Abrikosov, Calphad 32 (2008) 171–176.